Dalton Transactions

PAPER

View Article Online
View Journal | View Issue

Cite this: *Dalton Trans.*, 2014, **43**, 1025

Facile hydrothermal synthesis of TiO_2–Bi_2WO_6 hollow superstructures with excellent photocatalysis and recycle properties†

Ya-Fei Hou,[a,b] Shu-Juan Liu,*[a,b] Jing-huai Zhang,[c] Xiao Cheng[a,b] and You Wang*[a,b]

Received 28th July 2013,
Accepted 1st October 2013

DOI: 10.1039/c3dt52046c

www.rsc.org/dalton

One-dimensional mesoporous TiO_2–Bi_2WO_6 hollow superstructures are prepared using a hydrothermal method and their photocatalysis and recycle properties are investigated. Experimental results indicate that anatase TiO_2 nanoparticles are coupled with hierarchical Bi_2WO_6 hollow tubes on their surfaces. The TiO_2–Bi_2WO_6 structure has a mesoporous wall and the pores in the wall are on average 21 nm. The hierarchical TiO_2–Bi_2WO_6 heterostructures exhibit the highest photocatalytic activity in comparison with P25, pure Bi_2WO_6 hollow tube and mechanical mixture of Bi_2WO_6 tube and TiO_2 nanoparticle in the degradation of rhodamine B (RhB) under simulated sunlight irradiation. The as-prepared TiO_2–Bi_2WO_6 heterostructures can be easily recycled through sedimentation and they retains their high photocatalytic activity during the cycling use in the simulated sunlight-driving photodegradation process of RhB. The prepared mesoporous TiO_2–Bi_2WO_6 with hollow superstructure is therefore a promising candidate material for water decontamination use.

1. Introduction

The large scale application of sunlight-driven photocatalytic processes for water decontamination is dictated to a great extent by the semiconductor's stability and excellent photocatalytic property under solar light, as well as its simple and convenient recycle ability.[1,2] TiO_2 is the most widely investigated photocatalyst because of its high efficiency, good photostability, non-toxicity and low cost.[3–5] However, the wide band gap of TiO_2 (3.2 eV) limits its activation to ultraviolet irradiation, which is only 4% of the sunlight's energy reaching the earth's surface.[6] In order to efficiently utilize the full-band solar energy it is of great significance to develop a photocatalyst by coupling TiO_2 with a narrow band gap semiconductor such as an Aurivillius based compound.[7–9] Among these, Bi_2WO_6 with a band gap of 2.8 eV has emerged as a promising candidate due to its excellent visible-light-active photocatalytic activity for degradation of organic compounds.[10–12] On one hand, the TiO_2–Bi_2WO_6 heterostructure enables illumination from UV to visible light to be effectively utilized.[13] On the other hand, the synergetic effect between TiO_2 and Bi_2WO_6 can make the photogenerated electrons and holes be separated more efficiently, which leads to excellent photocatalytic property.[14–16]

Much work has been done on the fabrication of TiO_2–Bi_2WO_6 heterojunctions for its potential excellent photocatalytic performance in recent years. For example, Wang *et al.* fabricated Bi_2WO_6/TiO_2 nanofibers using electrospinning technique by surface-decorating continuous TiO_2 fibers with Bi_2WO_6 nanoparticles.[17] Colón *et al.* and other groups have reported TiO_2 modified flower/sphere-like Bi_2WO_6, respectively.[13,18,19] Tan *et al.* reported the preparation of Bi_2WO_6/TiO_2 heterojunction films on glass substrates using a superhydrophilicity-assisted method.[20] And all the heterostructures reported exhibit an improved photocatalytic property compared with individual components of Bi_2WO_6 or TiO_2.

It is generally accepted that the property of a photocatalyst is closely related to its size, morphology, and structure. For example, a mesoporous or hollow structure can increase its surface area so as to provide more reaction sites and facilitate the transportation of organic compound molecules, both of which can result in excellent photocatalytic activity.[21–23] Meanwhile for the nanosized Bi_2WO_6, although high photocatalytic activity is shown due to its large surface area, it is too small to recycle after the photocatalytic reaction.[13–16] The preparation of hierarchical photocatalysts with nanocrystals as building

[a]*School of Materials Science and Engineering, Harbin Institute of Technology, Harbin 150001, China. E-mail: liusj0817@hit.edu.cn, y-wang@hit.edu.cn; Fax: +86-451-86402716; Tel: +86-451-86402716*
[b]*Key Laboratory of Micro-Systems and Micro-Structures Manufacturing, Ministry of Education, Harbin 150001, China*
[c]*Key Laboratory of Superlight Materials & Surface Technology, Ministry of Education, Harbin Engineering University, Harbin 150001, China*
†Electronic supplementary information (ESI) available. See DOI: 10.1039/c3dt52046c

blocks is therefore popular. On the one hand, the nano subunits with higher redox potentials as a result of the increase in band gap energy can help retain high photocatalytic activities;[24] on the other hand, the larger bulk sizes of superstructures allow easier separation and recycling of the materials.[25] To the best of our knowledge, all the TiO_2–Bi_2WO_6 superstructures reported, including Bi_2WO_6/TiO_2 nanofibrous mat[17] and flower/sphere-like structures,[13,18,19] are solid structures without mesoporosity. It is therefore of great importance to synthesize TiO_2–Bi_2WO_6 superstructures with distinctive mesoporous hollow characteristics for its promising enhanced properties.

In our previous work, the distinctive hierarchical Bi_2WO_6 hollow tubes with macro-mesoporous walls were prepared successfully.[26] Herein, the surfaces of one-dimensional hierarchical Bi_2WO_6 hollow tubes are modified with anatase TiO_2 using a simple hydrothermal treatment. It is shown through experiments that the prepared heterostructure exhibits a significantly enhanced photocatalytic activity in the degradation of Rhodamine B (RhB) under simulated sunlight irradiation. In addition, this hybrid photocatalyst can be easily reclaimed through a natural sedimentation without decreasing of the photocatalytic activity, the characteristics of which are essential for practical waste-water purification.

2. Experimental section

2.1 Chemicals

Analytical grade HNO_3, $Bi(NO_3)_3{\cdot}5H_2O$, oleic acid, *n*-heptane, acetone, NaOH, acetic acid, ethanol, $Na_2WO_4{\cdot}2H_2O$, and tetrabutyl titanate were purchased from Sinopharm Chemical Reagent Co. and used without further purification.

2.2 Preparation of hierarchical TiO_2–Bi_2WO_6 heterostructures

Bi_2WO_6 hollow tubes were prepared firstly using a reported method.[26] 150 mg of as-prepared Bi_2WO_6 hollow tubes was added into 12 mL of deionized water with 5 mL of diluted acetic acid solution (20 vol%) in a beaker. 1 mL of tetrabutyl titanate was added into the suspension mentioned above. After being stirred for 1 h, the suspension was sealed into a Teflon-lined autoclave and treated at 180 °C for 21 h. The autoclave was then cooled down to room temperature naturally. The resulting sample was collected, rinsed in deionized water and then dried at 60 °C in air. By tuning the concentration of tetrabutyl titanate, three samples with different molar ratio of TiO_2 to Bi_2WO_6 were prepared and denoted as TB1, TB2 and TB3. The molar ratios are 6 : 1, 4.5 : 1 and 7.5 : 1 for the samples of TB1, TB2 and TB3, respectively. The molar ratios mentioned here are calculated according to the initially added amount of tetrabutyl titanate and Bi_2WO_6. For comparison, isolated TiO_2 was also prepared *via* the same method above without addition of Bi_2WO_6 hollow tubes.

2.3 Photocatalytic tests

The photocatalytic activities of the hierarchical TiO_2–Bi_2WO_6 heterostructures were evaluated through the degradation of RhB under simulated sunlight irradiation using a 500 W Xe lamp (Institute of Electric Light source, Beijing). The reaction cell was placed in a sealed block box with its top open to provide irradiation. The system was maintained at 20 °C by circulating water. In each experiment, 50 mg of as-prepared photocatalyst was added into 100 mL of RhB solution (1×10^{-5} mol L^{-1}). Prior to illumination, the suspensions were stirred in the dark for 30 min to establish the adsorption–desorption equilibrium between photocatalyst and RhB. Then, the solutions were exposed to the simulated sunlight irradiation under stirring. At a given time interval, 5 mL of aliquots were sampled and centrifuged to remove the photocatalyst. The concentration of RhB was analyzed using a UV-Vis spectrophotometer (VARIAN Cary 50 conc).

2.4 Characterization

XRD pattern was recorded with a German BRUKER D8-ADVANCE with Cu Kα radiation (λ = 0.15406 nm) at 40 kV and 40 mA. Field-emission scanning electron microscope (FESEM) images were taken on a field emission scanning electron microscope (Sirion 200) at an acceleration voltage of 10 kV. Transmission electron microscope (TEM) images, high-resolution transmission electron microscope (HRTEM) images, and selected area electron diffraction (SAED) patterns were taken on a JEOL 2100 microscope at an accelerating voltage of 300 kV. UV-Vis diffuse reflectance spectra (DRS) were established using a UV-Vis spectrophotometer (Hitachi U-3100) with an integrating sphere accessory. Nitrogen adsorption–desorption measurements were made at 77 K on a Micromeritics Tristar 3000 analyzer after the samples were degassed at 150 °C for 6 h. Total organic carbon (TOC) was assayed on a Shimadzu TOC-5000A analyzer.

3. Results and discussion

3.1 Characterization of TiO_2–Bi_2WO_6 heterostructures

The hierarchical Bi_2WO_6 hollow tubes are prepared following the procedure we have previously developed.[26] Their detailed structure is shown in the FESEM and TEM images in Fig. 1. From the broken tube in Fig. 1b it can be seen that Bi_2WO_6 has a structure of hollow tubes with the walls made of numerous interlaced nanoplates. Further local magnification as shown in the top right inset shows that the surface of Bi_2WO_6 nanoplates is rather smooth.

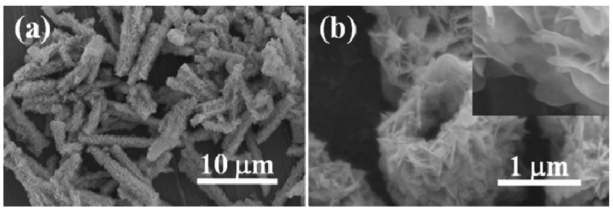

Fig. 1 FESEM and TEM images of Bi_2WO_6 prepared at 120 °C for 6 h. (a) Overall morphology; (b) close-up view of a broken tube.

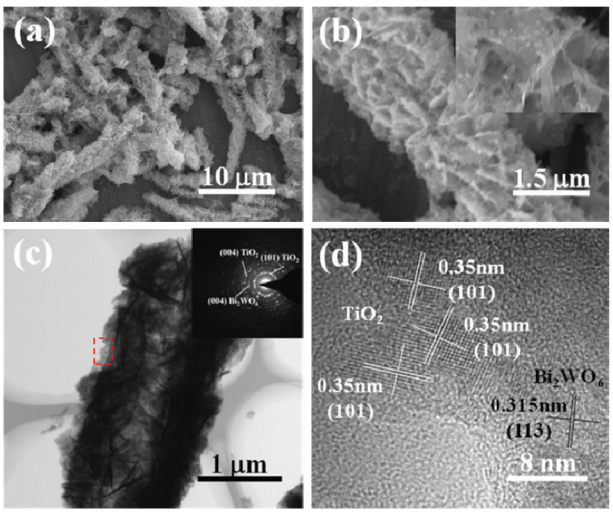

Fig. 2 FESEM, TEM and HRTEM images of typical TiO_2–Bi_2WO_6 heterostructures (sample TB1) prepared through hydrothermal treatment at 180 °C for 21 h.

Fig. 2a is a low-magnification FESEM image of typical TiO_2–Bi_2WO_6 heterostructure hollow tubes (sample TB1). It can be seen by comparing Fig. 1a and 2a that the general morphology of 2 ± 0.5 μm in diameter and 9 ± 4 μm in length remain almost unchanged before and after TiO_2 modification. The close-up view of tubes in Fig. 2b indicates that after hydrothermal treatment many TiO_2 nanoparticles are attached to the previously smooth surface of a Bi_2WO_6 nanoplate. As shown in Fig. 2c the hollow nature of the modified tubes can be clearly seen and the diffraction rings of the SAED pattern taken at the outmost layer of the tubes can be indexed to a mixture of orthorhombic Bi_2WO_6 and anatase TiO_2, which confirms our deduction that the attached nanoparticles are indeed TiO_2. The corresponding HRTEM image from the heterostructures displays two types of clear lattice fringes, as shown in Fig. 2d. One set of fringe spacing is *ca.* 0.35 nm, corresponding to the (101) plane of anatase crystal structure of TiO_2. The other set of fringes with spacing of *ca.* 0.315 nm corresponds to the (113) lattice spacing of the orthorhombic phase of Bi_2WO_6.

Further evidence comes from the XRD pattern of the as-prepared TB1 sample as shown in Fig. 3. It can be seen that the diffraction peaks of anatase TiO_2 (JCPDS card no. 21-1272) and orthorhombic Bi_2WO_6 (JCPDS card no. 73-1126) coexist in the sample, which shows the formation of a TiO_2–Bi_2WO_6 heterostructure. Moreover, no diffraction peaks of other phases are observed, which means the modified TiO_2 phase has no effect on the pre-existing Bi_2WO_6. Comprehensively considering the results of FESEM, SAED, HRTEM and XRD, it can be concluded that a TiO_2–Bi_2WO_6 heterostructure with TiO_2 nanoparticles attached on the surface of Bi_2WO_6 hollow tubes has been fabricated successfully.

The porosity of the TiO_2–Bi_2WO_6 heterostructure is investigated by N_2 adsorption–desorption isotherms (Fig. 4) and the corresponding BJH pore size distribution plot is shown in the inset.[27] A narrow pore size distribution centering on 21 nm is

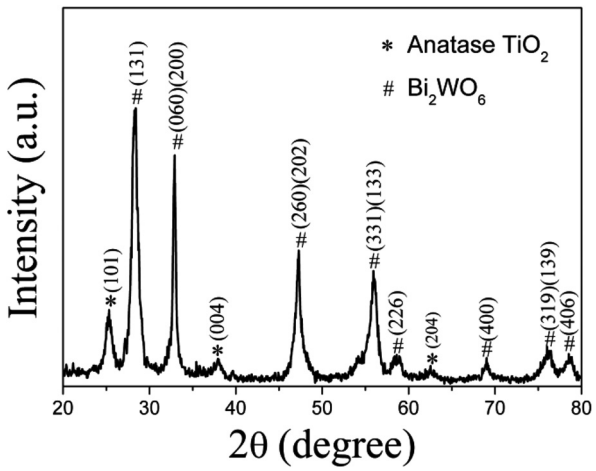

Fig. 3 XRD pattern of sample TB1 prepared at 180 °C for 21 h.

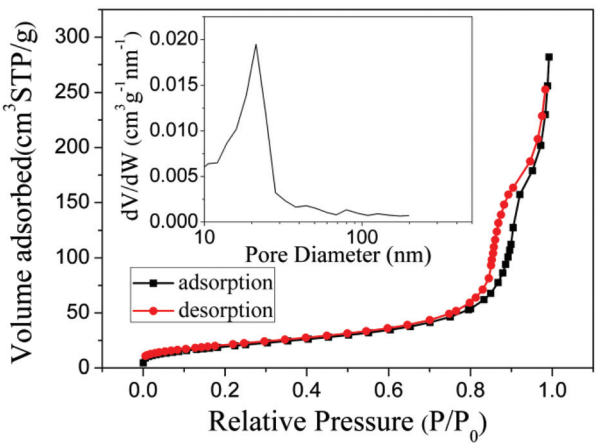

Fig. 4 Nitrogen adsorption–desorption isothermal and pore size distribution curve (insert) of TiO_2–Bi_2WO_6 heterostructure (sample TB1).

observed, indicating that the mesoporous characteristic of the Bi_2WO_6 hollow tubes is retained by the heterostructure after TiO_2 is attached to the surface. In comparison with the pore size distribution of Bi_2WO_6 hollow tubes with several peaks ranging from 2 to 100 nm, the decoration of TiO_2 nanoparticles narrows the pore size distribution significantly. More importantly, as shown in Table 1, the measured Brunauer–Emmett–Teller (BET) surface areas of TB1, TB2 and TB3 are greatly enhanced compared with that of Bi_2WO_6 hollow tubes. The observed increase in BET surface area as a result of TiO_2 modification is in agreement with what is reported in the literature.[28] The hierarchical mesoporous structure and the larger BET surface area not only facilitate the absorption and utilization of sunlight but also improve the contact of photocatalysts with organic contaminants. Therefore, a

Table 1 BET surface areas of samples prepared

Samples	P25	TB1	TB2	TB3	TiO_2	Bi_2WO_6
BET surface area ($m^2\ g^{-1}$)	50	72	54	129	156	32

structure associated enhancement can be expected in the photocatalytic activity of prepared TiO_2–Bi_2WO_6.

3.2 Influencing factors on the formation of TiO_2–Bi_2WO_6

To obtain an optimal composition for the coupling of TiO_2 with Bi_2WO_6, control experiments are made by adding different amounts of tetrabutyl titanate. The influence of the molar ratio of TiO_2 to Bi_2WO_6 on the resulting morphology is displayed in Fig. 5. As shown in Fig. 5a, very few TiO_2 nanoparticles are attached to the surfaces of Bi_2WO_6 tubes when the ratio is kept at 4.5 : 1 (sample TB2). When the ratio increases to 6 : 1 (sample TB1), it can be seen from Fig. 2b that TiO_2 nanoparticles are evenly distributed on the Bi_2WO_6 surfaces with little surplus left on the substrate. Further increasing the ratio to 7.5 : 1 (sample TB3), TiO_2 nanoparticles are over-loaded on the Bi_2WO_6 surfaces and many surplus nanoparticles are scattered on the substrate (see Fig. 5b). Unless otherwise mentioned, 6 : 1 is used as the typical ratio for the studies.

The time-dependent influence on the phase composition of photocatalysts is also investigated. As shown in Fig. S1,† in the initial period of reaction (1 h), no anatase TiO_2 phase can be observed in the XRD pattern. After the reaction lasts for 7 h, crystalline anatase TiO_2 is found in the product. When the reaction time is prolonged from 14 h to 28 h, no obvious phase changes can be observed in the corresponding XRD patterns, which means that reaction time longer than 14 h will not affect the final phase composition of the sample. Further experiments on the photocatalytic performance in the following section suggest that the photocatalytic activity of TiO_2–Bi_2WO_6 heterostructures can be influenced by the reaction time of photocatalysts.

3.3 Optical properties and photocatalytic performance

3.3.1 Optical properties. It is generally known that the optical properties of a semiconductor, which mainly include energy level and band gap, are key factors in determining its phototocatalytic activities.[29] Fig. 6 shows the UV-Vis diffuse reflectance spectra of TiO_2 nanoparticles, Bi_2WO_6 and as-prepared TiO_2–Bi_2WO_6 hierarchical heterostructures. It can be seen from Fig. 6 that the TiO_2 nanoparticles have photo-absorption mainly in the UV region and the photo-absorption of Bi_2WO_6 covers from UV to visible light regions. Compared to that of single TiO_2 and Bi_2WO_6, the absorption of the TiO_2–Bi_2WO_6 heterostructure appears an enhanced optical

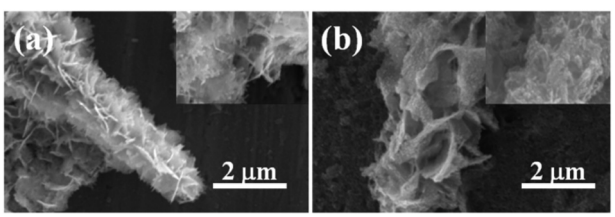

Fig. 5 FESEM images of TiO_2–Bi_2WO_6 heterostructures with different molar ratios of TiO_2 to Bi_2WO_6 (a) 4.5 : 1 (sample TB2), (b) 7.5 : 1 (sample TB3).

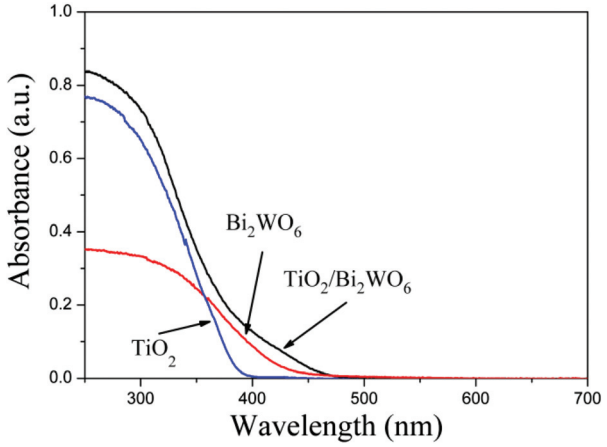

Fig. 6 UV-Vis diffuse reflectance spectra of TiO_2, Bi_2WO_6 and TiO_2–Bi_2WO_6 heterostructures.

absorption both in the UV and visible regions. An obvious red shift toward the visible light region can be observed and charge-transfer transitions between TiO_2 and Bi_2WO_6 conduction or valence in the hybrid sample should be the main reason.[30] According to the equation of $\alpha h\nu = A(h\nu - E_g)^{1/2}$, where α, h, ν, A and E_g are absorption coefficient, Planck's constant, frequency of vibration, proportional constant and band gap, respectively,[31,32] the band gap of pure Bi_2WO_6 and TiO_2 is calculated to be 2.85 eV and 3.2 eV, respectively, while that of the TiO_2–Bi_2WO_6 heterostructures is 2.71 eV. The decreased band gap of the hybrid means that more UV-visible light with low energy can stimulate the photocatalyst to generate electron–hole pairs. Therefore a better photocatalytic performance of the hybrid can be expected under simulated sunlight irradiation.

To prove the photocatalytic activity of prepared TiO_2–Bi_2WO_6 heterostructures, RhB is chosen as the target pollutant and its characteristic absorption band at 553 nm is employed to monitor the degradation process. The photodegradation efficiencies of RhB over P25, the mechanically mixed TiO_2 and Bi_2WO_6, as well as TB1, TB2 and TB3 samples with different TiO_2 content under simulated sunlight irradiation are shown in Fig. 7. It can be seen from Fig. 7 that almost no degradation of RhB occurs in the absence of photocatalyst after being irradiated for 60 min, which indicates the significance of photocatalyst (Curve A). The Bi_2WO_6 hollow tubes show a photocatalytic efficiency of 80% in 60 min, which is better than those of mechanically mixed TiO_2 and Bi_2WO_6 (66%) and P25 (62%). The better performance of Bi_2WO_6 hollow tubes can be attributed to the novel structure of porous tube wall and hollow interior which have more surface areas to react and more channels to facilitate the transmission of sunlight and diffusion of molecules. Due to the excellent properties of Bi_2WO_6 hollow tubes, all the composite photocatalysts (TB1, TB2 and TB3) exhibit better performance in degradation of RhB than those of either pure components or mechanically mixed ones. It can therefore be concluded that the photocatalytic activity of TiO_2–Bi_2WO_6 heterostructure is effectively enhanced by coupling.

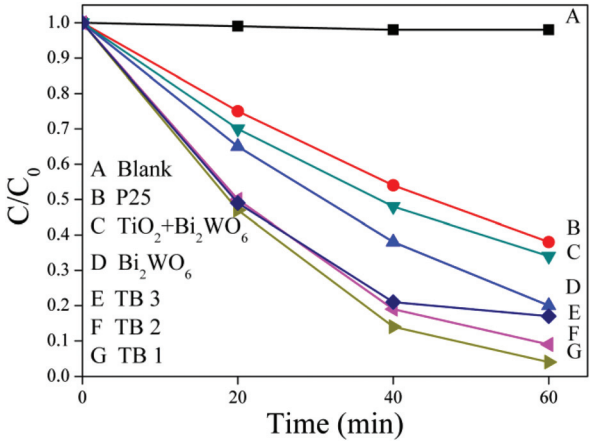

Fig. 7 Photocatalytic degradation of RhB under simulated sunlight irradiation with different samples: A, blank; B, P25; C, mechanically mixed TiO_2 and Bi_2WO_6; D, Bi_2WO_6 tubes; E, TB3; F, TB2; G, TB1.

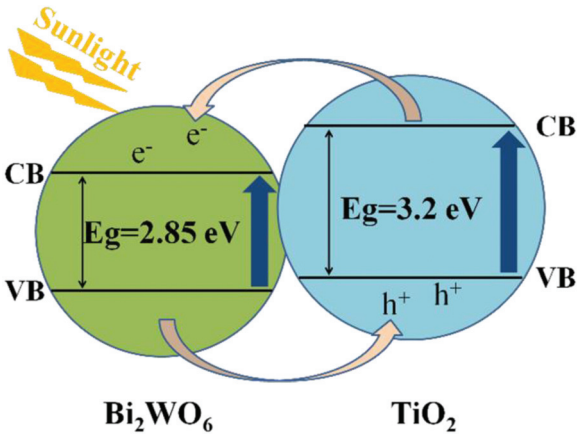

Fig. 8 Schematic diagram for energy band matching and electron–hole separation of TiO_2–Bi_2WO_6 heterostructure.[2,17,18,20]

Among the composite samples, TB1 with a molar ratio of TiO_2 to Bi_2WO_6 of 6 : 1 exhibits the best photocatalytic activity, and the degradation efficiency of RhB reaches 96% in 60 min (curve G). Samples exhibit decreased photocatalytic activity when the ratio is below or above 6 : 1. Combining Table 1 and Fig. 7, it can be seen that although TB3 has the largest BET surface area, its photocatalytic activity is the worst of the three composites. These results indicate that although larger BET surface area is beneficial for the improvement of photocatalytic performance, it is not the decisive factor for the composites here. The synergetic effect in the heterostructures, which can increase the life of photogenerated electrons and holes efficiently, plays a more important role here. Thus, to effectively use the synergetic effect, an optimal loading of TiO_2 on Bi_2WO_6 is pivotal for producing TiO_2 sensitized Bi_2WO_6 composite with high activity. When the loading amount of TiO_2 is low the separation efficiency of electron–hole pairs will not be high enough and the photocatalytic activity can not reach the maximum. However, overlapping agglomerates would smother the surface of Bi_2WO_6 if the TiO_2 amount is too high. Subsequently the electron transfer across the interfaces of hierarchical TiO_2–Bi_2WO_6 heterostructure is partially hindered by excess TiO_2, which leads to a decreased photocatalytic property.

Moreover, photocatalytic activities of the samples taken at different reaction times are investigated (Fig. S2†). It is obvious that the reaction time has a significant effect on the photocatalytic activity of the as-prepared samples. In the initial stage, longer reaction time helps the improvement of photocatalytic activity. Optimum photocatalytic performance can be obtained when the reaction time reaches 21 h. On the contrary, reaction for more than 21 h will lead to a decrease in the performance. Considering the photocatalytic performances of the hybrids, 21 h is therefore selected as the reaction time for preparation of TiO_2–Bi_2WO_6 heterostructures.

3.3.2 Photocatalytic mechanism. To thoroughly understand the mechanism, total organic carbon (TOC) analysis was carried out on the RhB solution before and after photocatalytic reactions. Taking TB1 as an example, TOC of its RhB solution dropped from 3.36 mg L^{-1} to 1.82 mg L^{-1}, which proves the degradation of RhB while not just due to photosensitization. The generation of other organic compounds under the photocatalytic process[33–35] would be the main reason for the still larger TOC.

From the photocatalytic results above, it is evident that the heterojunction formed in the TiO_2–Bi_2WO_6 hybrids is responsible for its improved photocatalytic performance under simulated sunlight excitation. A clear synergetic mechanism according to the conductor band (CB) and valence band (VB) edge potentials of TiO_2 and Bi_2WO_6 as reported by others[2,17,18,20] is displayed in Fig. 8. Under simulated sunlight irradiation, both TiO_2 and Bi_2WO_6 can be excited to generate electron–hole pairs. The electrons in the CB of TiO_2 can easily flow to the CB edge of Bi_2WO_6 through the interface because the CB edge of TiO_2 is more negative than that of Bi_2WO_6. On the other hand, the holes in the VB of Bi_2WO_6 can be transferred to the VB of TiO_2 considering that the VB edge level of Bi_2WO_6 is more positive than that of TiO_2. The photogenerated electrons and holes can thus be effectively separated at the interface of TiO_2–Bi_2WO_6, and then migrate to the surface of the photocatalyst.[18,36] A larger number of electrons in the Bi_2WO_6 surface and holes in the TiO_2 surface can participate in the photocatalytic reaction to directly or indirectly mineralize organic pollutants, and the photocatalytic reaction can thus be greatly enhanced.

3.3.3 Cycling use. In order to ensure the long-term practical application of a photocatalyst, the following two aspects need to be considered: (i) the ease with which the photocatalyst can be separated from the solution; (ii) the stability of the photocatalyst to maintain its high activity over time.[37] Considering the above, natural settlement experiments after completion of photodegradation are performed. As shown in Fig. 9 it can be seen that the hierarchical TiO_2–Bi_2WO_6 photocatalyst can settle naturally in 30 min, which means this heterostructure is very easy to recycle. In comparison, almost no

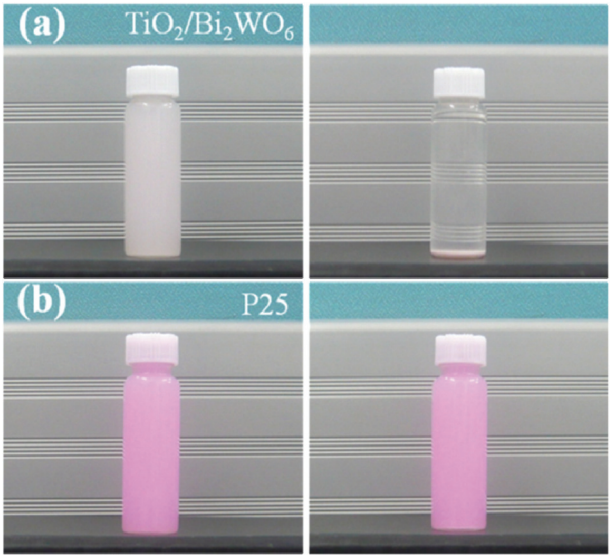

Fig. 9 Natural settlement for 30 min after photodegradation of different photocatalysts: (a) TiO_2–Bi_2WO_6 (b) P25.

P25 can precipitate in such a short period of time and very few photocatalysts can settle naturally even in one day and only with a high-speed centrifugation can they be separated. On the other hand, the stability of the high photocatalytically performing TiO_2–Bi_2WO_6 heterostructure is verified by cycling TiO_2–Bi_2WO_6 for the photocatalytic degradation of RhB under simulated sunlight irradiation as shown in Fig. 10. After every photodegradation run of 60 min, the photocatalyst is separated, washed with deionized water and dried. Upon completion of seven cycles, there is no significant loss in photocatalytic activity, which implies that the photocatalytic property of the TiO_2–Bi_2WO_6 heterostructure is generally stable in the whole photocatalytic process. Thus, the excellent photocatalytic activity and easy recycling property of the hierarchical TiO_2–Bi_2WO_6 hollow heterostructure enable it to have great potential for a long term practical application.

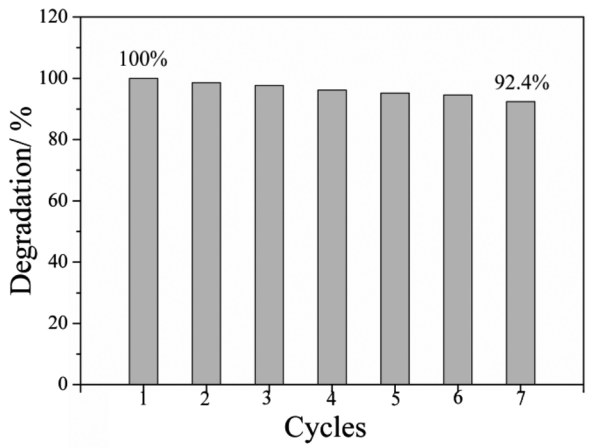

Fig. 10 Cycling runs of photocatalytic degradation of RhB in presence of TiO_2–Bi_2WO_6 heterostructures under simulated sunlight irradiation.

4. Conclusion

In summary, a novel hierarchical TiO_2–Bi_2WO_6 hollow heterostructure with excellent photocatalysis and recycling properties is successfully prepared using a hydrothermal process. It is found that TiO_2 nanoparticles are modified on the surface of hierarchical Bi_2WO_6 hollow tubes and the heterostructure has a mesoporous characteristic with the pore size distribution centering on 21 nm. The hollow and porous TiO_2–Bi_2WO_6 superstructure possesses favorable recycling characteristics and excellent photostability, and exhibits an enhanced photocatalytic activity in the decomposition of RhB under simulated sunlight irradiation. The enhanced photocatalytic activity can be attributed to the synergetic effect providing the efficient separation and recombination preventing of electron–hole pairs, high surface area creating more catalytic sites, and porous characteristics facilitating the transmission of simulated sunlight and diffusion of molecules. These results indicate that the hierarchical TiO_2–Bi_2WO_6 hollow heterostructure is a promising candidate material for wastewater treatment for its enhanced photocatalysis and recycling properties.

Acknowledgements

This work is funded by National Natural Science Foundation of China (21101043), Natural Science Foundation of Heilongjiang Province of China (Key Program) under Grant ZD20080201, Excellent Youth Foundation of Heilongjiang Province of China under Grant JC200902, Research Fund for Doctoral Program of Higher Education of China (20112302120018), Natural Science Foundation of Heilongjiang Province of China (QC2010032), Fundamental Research funds for Central Universities (HIT.KLOF.2010009), Special Research funds for Scientific and Technical Innovative Talents of Harbin City (2012RFQXG108) and China Postdoctoral Science Foundation (20100471046).

Notes and references

1 X. B. Chen, L. Liu, P. Y. Yu and S. S. Mao, *Science*, 2011, **331**, 746.
2 M. Shang, W. Z. Wang, L. Zhang, S. M. Sun, L. Wang and L. Zhou, *J. Phys. Chem. C*, 2009, **113**, 14727.
3 J. J. Zou, H. He, L. Cui and H. Y. Du, *Int. J. Hydrogen Energy*, 2007, **32**, 1762.
4 Y. Zhou, F. Krumeich, A. Heel and G. R. Patzke, *Dalton Trans.*, 2010, **39**, 6043.
5 J. J. Zou, B. Zhu, L. Wang, X. W. Zhang and Z. T. Mi, *J. Mol. Catal. A: Chem.*, 2008, **286**, 63.
6 L. S. Zhang, H. L. Wang, Z. G. Chen, P. K. Wong and J. S. Liu, *Appl. Catal., B*, 2011, **106**, 1.
7 G. H. Tian, Y. J. Chen, W. Zhou, K. Pan, Y. Z. Dong, C. G. Tian and H. G. Fu, *J. Mater. Chem.*, 2011, **21**, 887.
8 L. Zhang, D. R. Chen and X. L. Jiao, *J. Phys. Chem. B*, 2006, **110**, 2668.
9 J. C. Yu, L. Wu, J. Lin, P. S. Li and Q. Li, *Chem. Commun.*, 2003, 1552.

10 F. Amano, K. Nogami, M. Tanaka and B. Ohtani, *Langmuir*, 2010, **26**, 7174.
11 F. Amano, K. Nogami, R. Abe and B. Ohtani, *J. Phys. Chem. C*, 2008, **112**, 9320.
12 L. S. Zhang, W. Z. Wang, Z. G. Chen, L. Zhou, H. L. Xu and W. Zhu, *J. Mater. Chem.*, 2007, **17**, 2526.
13 Y. Zheng, K. L. Lv, X. F. Li, K. J. Deng, J. Sun, L. Q. Chen, L. Z. Cui and D. Y. Du, *Chem. Eng. Technol.*, 2011, **34**, 1630.
14 L. M. Wang, N. Wang, L. H. Zhu, H. W. Yu and H. Q. Tang, *J. Hazard. Mater.*, 2008, **152**, 93.
15 X. W. Wang, G. Liu, Z. G. Chen, F. Li, L. Z. Wang, G. Q. Lu and H. M. Cheng, *Chem. Commun.*, 2009, 3452.
16 Y. Z. Lei, G. H. Zhao, M. C. Liu, Z. N. Zhang, X. L. Tong and T. C. Cao, *J. Phys. Chem. C*, 2009, **113**, 19067.
17 Y. P. Zhang, L. F. Fei, X. D. Jiang, C. X. Pan and Y. Wang, *J. Am. Ceram. Soc.*, 2011, **94**, 4157.
18 G. Colón, S. M. Lopez, M. C. Hidalgo and J. A. Navio, *Chem. Commun.*, 2010, **46**, 4809.
19 S. Murcia-Lopez, M. C. Hidalgo and J. A. Navio, *Appl. Catal., A*, 2012, **423**, 34.
20 Q. C. Xu, D. V. Wellia, Y. H. Ng, R. Amal and T. T. Y. Tan, *J. Phys. Chem. C*, 2011, **115**, 7419.
21 Y. Y. Li, J. P. Liu and X. T. Huang, *Nanoscale Res. Lett.*, 2008, **3**, 365.
22 Y. Huang, Z. H. Ai, W. K. Ho, M. J. Chen and S. Lee, *J. Phys. Chem.C*, 2010, **114**, 6342.
23 J. Q. Li, Z. Y. Guo, H. G. Yu, H. Liu, D. F. Wang and Z. F. Zhu, *Micro Nano Lett.*, 2012, **7**, 52.
24 M. Ge, Y. F. Li, L. Liu, Z. Zhou and W. Chen, *J. Phys. Chem. C*, 2011, **115**, 5220.
25 J. S. Hu, L. L. Ren, Y. G. Guo, H. P. Liang, A. M. Cao, L. J. Wan and C. L. Bai, *Angew. Chem., Int. Ed.*, 2005, **44**, 1269.
26 S. J. Liu, Y. F. Hou, S. L. Zheng, Y. Zhang and Y. Wang, *CrystEngComm*, 2013, **15**, 4124–4130.
27 Q. Zhang, W. Y. Chi, W. W. Zhang, C. Y. Lv and J. X. Li, *New J. Chem.*, 2012, **36**, 119.
28 M. S. P. Francisco, V. R. Mastelaro, P. A. P. Nascente and A. O. Florentino, *J. Phys. Chem. B*, 2001, **105**, 10515.
29 K. Nagaveni, M. S. Hegde, N. Ravishankar, G. N. Subbanna and G. Madras, *Langmuir*, 2004, **20**, 2900.
30 L. Ge and J. Liu, *Appl. Catal., B*, 2011, **105**, 289.
31 J. W. Tang, Z. G. Zou and J. H. Ye, *J. Phys. Chem. B*, 2003, **107**, 14265.
32 J. Yin, Z. G. Zou and J. H. Ye, *J. Phys. Chem. B*, 2003, **107**, 4936.
33 X. F. Cao, L. Zhang, X. T. Chen and Z. L. Xue, *CrystEngComm*, 2011, **13**, 306–311.
34 H. B. Fu, C. S. Pan, W. Q. Yao and Y. F. Zhu, *J. Phys. Chem. B*, 2005, **109**, 22342–22439.
35 F. Duan, Y. Zheng and M. Q. Chen, *Mater. Lett.*, 2011, **65**, 191–193.
36 Y. Y. Li, J. P. Liu, X. T. Huang and J. G. Yu, *Dalton Trans.*, 2010, **39**, 3420.
37 M. Y. Zhang, C. L. Shao, J. B. Mu, Z. Y. Zhang, Z. C. Guo, P. Zhang and Y. C. Liu, *CrystEngComm*, 2012, **14**, 605.